CCFE
CULHAM CENTRE FOR FUSION ENERGY

UK Atomic Energy Authority

UKAEA-CCFE-PR(19)61

D. Patel, M.D. Richardson, B. Jim, S. Akhmadaliev, R. Goodall, A.S. G, y

Radiation Damage Tolerance of a Novel Metastable Refractory High Entropy Alloy V2.5Cr1.2WMoCo0.04

Radiation Damage Tolerance of a Novel Metastable Refractory High Entropy Alloy V2.5Cr1.2WMoCo0.04

D. Patel, M.D. Richardson, B. Jim, S. Akhmadaliev, R. Goodall, A.S. G, y

This is a preprint of a paper submitted for publication in Journal of Nuclear Materials

Radiation Damage Tolerance of a Novel Metastable Refractory High Entropy Alloy $V_{2.5}Cr_{1.2}WMoCo_{0.04}$

Dhinisa Patel[1*], Mark D. Richardson[2], Bethany Jim[1,3], Shavkat Akhmadaliev[4], Russell Goodall[1], Amy S. Gandy[1]

[1]Department of Materials Science and Engineering, University of Sheffield, S1 3JD, UK

[2]United Kingdom Atomic Energy Authority, Culham Centre for Fusion Energy, Culham Science Centre, Abingdon, Oxfordshire, OX14 3DB, UK

[3]Department of Materials, University of Oxford, Parks Road, Oxford, OX1 3PH, UK

[4]Institute of Ion Beam Physics and Materials Research, Helmholtz Zentrum Dresden-Rossendorf, Dresden 01328, Germany

[*]**Correspondence:**

Dhinisa Patel

ddpatel1@sheffield.ac.uk

Abstract

A novel multicomponent alloy, $V_{2.5}Cr_{1.2}WMoCo_{0.04}$, produced from elements expected to favour a BCC crystal structure, and to be suitable for high temperature environments, was fabricated by arc melting and found to exhibit a multiphase dendritic microstructure with W-rich dendrites and V-Cr segregated to the inter-dendritic cores. The as-cast alloy displayed an apparent single-phase XRD pattern. Following heat treatment at 1187 °C for 500 hours the alloy transformed into three different distinct phases - BCC, orthorhombic, and tetragonal in crystal structure. This attests to the BCC crystal structure observed in the as-cast state being metastable. The radiation damage response was investigated through room temperature 5 MeV Au^+ ion irradiation studies. Metastable as-cast $V_{2.5}Cr_{1.2}WMoCo_{0.04}$ shows good resistance to radiation induced damage up to 40 displacements per atom (dpa). 96 wt% of the as-cast single-phase BCC crystal structure remained intact, as exhibited by grazing incidence X-ray diffraction (GI-XRD) patterns, whilst the remainder of the alloy transformed into an additional BCC crystal structure with a similar lattice parameter. The exceptional phase stability seen here is attributed to a combination of self-healing processes and the BCC structure, rather than a high configurational entropy, as has been suggested for some of these multicomponent "High Entropy Alloy" types. The importance of the stability of metastable high entropy alloy phases is for the first time highlighted and the findings thus challenge the current understanding of phase stability after irradiation of systems like the HEAs.

Introduction

Initially detailed by Yeh et al. (2004) and Cantor et al. (2004), high entropy alloys (HEAs) are described as multi-component metallic systems with no principal element. Sometimes termed multicomponent concentrated solid-solution alloys (CSAs) they are defined as alloys with five or more alloying elements present either equiatomically, or in the range of 5-35 at %, offering a wide range of possible HEAs. Typically, HEAs have been proposed for use as structural applications due to their superior mechanical properties, including high hardness and wear resistance (Huang et al., 2004 and Chuang et al., 2011), high temperature (Senkov et al., 2014) and corrosion resistance; it is these properties which make HEAs attractive for applications in extreme environments. The high configurational entropy of these alloys has been proposed to encourage the formation of solid solutions consisting of simple body-centered cubic (BCC) or face-centered cubic (FCC) crystal structures rather than the more highly ordered intermetallic phases. For extreme environments, including high temperature and heavy neutron bombardment, the formation of undesirable phases during exposure to operational temperatures would likely result in a decline of mechanical performance potentially to an inoperable level. At elevated temperatures the high mixing entropy decreases the Gibbs free energy of the system and so greatly contributes to the stability of single-phase HEAs, but this effect bears less significance at lower temperatures. Additionally, enthalpy can also lead to phase separation even at high mixing entropy states (Wei et al, 2018). Exploration of the temperature-dependent metastability of HEAs has shown to sometimes result in enhanced toughness, ductility, and strength.

For example, upon quenching, non-equiatomic $Fe_{50}Mn_{30}Co_{10}Cr_{10}$ undergoes a partial martensitic transformation to HCP from room temperature stable FCC, resulting in an increase of ductility and strength (Li et al, 2016).

HEAs have been reported to exhibit a self-healing process (Egami et al., 2014) during energetic ion implantation, due to the proposed high formation energies of vacancies and interstitials in HEAs induced by the local atomic-level stresses. HEAs are thought to have high atomic-stresses, in comparison to conventional alloys, due to the large differences in atomic sizes of the elements incorporated in the lattice (He and Yang, 2018). Upon ion implantation, particle bombardment initiates atomic displacement and prompts large thermal spikes allowing the relaxation and recovery of the Frenkel pairs. This results in high recombination of defects to decrease strain, leaving the alloy with significantly fewer defects than conventional materials, and thus restrains the formation of dislocation loops and voids (Xia et al., 2015). Irradiation-induced defects lead to structural damage in materials and so the self-healing effect is another feature making HEAs an attractive candidate for fission and fusion-based nuclear reactors (Liaw et al., 2015).

Recent studies have reported the radiation response of some HEAs (Kombaiah et al., 2018; Kumar et al., 2016; Xia et al., 2015) where many of these studies have been for homogenised single-phase alloys. Studies regarding the phase stability of HEAs after irradiation mostly focus on single-phase FCC crystalline structures with many revolving around relatively minor variations to the content and composition of CrMnFeCoNi, "Cantor's alloy" (Lu et al., 2018; He et al., 2017; Xia et al., 2015) and therefore concentrating on the 3d transition metals. For materials exposed to irradiation by heavy energy particles, BCC-structured materials are generally preferred over those with an FCC crystal structure as they are more radiation damage-tolerant. This is likely due to the enhanced formation of small defect clusters and finely dispersed point defects in non-close-packed BCC materials as opposed to the larger, less mobile defect clusters seen in FCC materials. Smaller defect clusters enhance the probability of vacancy-interstitial recombination upon ion implantation, thus reducing irradiation-induced structural changes in materials (Zinkle, 2005). When considering materials for radiation damage resistance, phase changes during service are of concern as they are likely to alter the microstructure of the alloy, thus affecting the in-service mechanical performance.

Conventional multiphase alloys subjected to ion implantation have been studied to determine their response in extreme environments. It is known for multiphase alloys that upon ion implantation the second-phase precipitates undergo a series of complex processes simultaneously including: disordering or amorphisation, radiation enhanced diffusion, and irradiation-induced solute segregation (Li et al., 2015). Alternatively, in nano-structured alloys irradiation generally leads to the formation of precipitates. Nano-structured Cu-based alloys, $Cu_{93.5}W_{6.5}$ and $Cu_{99}W_1$, upon 1.8 MeV Kr^+ irradiation resulted in the uniform distribution of W-rich nano-precipitates. The absence of nano-precipitates after thermal annealing implies the formation of nano-precipitates occurred during the thermal spike phase of the cascade evolution (Tai et al., 2012 and 2014). It has been shown that nanoscale precipitates serve as point defect recombination sites and so are an effective way of minimising remaining defects at high temperatures (Zinkle, 2005).

There is a clear need therefore to explore the effectiveness of multiphase HEAs against radiation damage. This sentiment is echoed by both Miracle et al. (2014) and Liaw et al. (2015) who advise against the sole pursuit of single-phase solid solution alloys and instead suggest intentionally adding secondary phases to examine the efficacy of particle strengthening of HEAs which can be more effective at higher temperatures than other classical strengthening mechanisms (work-hardening, solid solution strengthening, grain boundary strengthening).

The Single-Phase High Entropy Alloy (SP-HEA) 31.3Cr-23.6Mo-26.4V-18.7W (termed CrMoVW) was recently fabricated and characterised in the as-cast state for application in high temperature, oxidising environments (Ikeuchi et al., 2019). The composition was determined through Density Functional Theory (DFT) studies and the Alloy Search and Predict (ASAP) method to maximise the alloy melting temperature whilst also maintaining a single phase below the solidus. Refractory elements were chosen for their high melting temperatures (and then ranked by low cost) as well as an addition of Cr to prevent oxide scale formation. The binary phase diagrams of the elements all indicate formation of a BCC solid solution over a wide temperature range and across a variety of compositions with no apparent binary intermetallic compounds. All the elemental crystal structures are BCC-structured over a wide range of temperatures which further promotes the stability of a BCC solid solution. In the current work, to reduce the elemental segregation displayed by the alloys fabricated by Ikeuchi et al. (formed by large differences in the melting temperatures of the components), refinement of the alloy composition and amendment of the arc-melting process were undertaken. The alloy design process was achieved by utilising a combination of the CALPHAD method and the thermodynamic parameters used for prediction of solid solution for high entropy alloys (Gandy et al., 2019) resulting in the prediction of a novel alloy of nominal composition $V_{2.5}Cr_{1.2}WMo$. To avoid the only partial melting of the MoVW phase observed in the CrMoVW alloy, all constituents were melted together with the highest melting temperature elements covering the lowest melting

temperature elements. Additional Cr was added to the elemental mix to account for its low boiling point and subsequent partial evaporation during fabrication. To explore the microstructural and elemental distribution changes after irradiation this alloy was characterised in the as-cast state and after room temperature Au^+ ion implantation, and to assess thermal stability the alloy was annealed at intermediate temperature (1187 °C) for 500 hours.

The key aim of this study is to evaluate whether multiphase HEAs possess the same phase stability as single-phase HEAs. Many alloys described as HEAs do not have a single-phase structure, and this is particularly true of those based on the refractory elements (Huang et al., 2017; Fazakaz et al., 2014; Guo et al., 2016). This could be significant for radiation damage resistance as, on the atomic-scale where incident particles are interacting with the material, potentially inducing damage, the local environment of the atoms in a multiphase structure will be significantly different and potentially much less disordered and therefore less likely to benefit from some of the suggested inherent advantages to HEAs. However, in contrast to recent research we find that the multiphase nature does not negatively impact the radiation damage response, therefore suggesting an alternative mechanism to configurational entropy stability.

Materials and Methods

Alloy Design

Efforts have been made to quantitatively predict alloy composition with a single-phase solid solution (Takeuchi and Inoue, 2000 and 2005; Zhang et al., 2008). Thermodynamic parameters derived and extrapolated from the Hume-Rothery rules include atomic size difference and heat of mixing of binary pairs which were proposed by Takeuchi and Inoue (2000) for the formation of bulk metallic glasses (BMGs). This advance of the understanding of formation of BMGs (Takeuchi and Inoue, 2005) also helped high entropy alloy design.

Zhang et al. (2008) identified atomic and thermodynamic parameters which could give the likelihood of the formation of solid solution systems, specifically for multicomponent alloys. They included previous terms such as atomic size difference, mixing enthalpy of a solid solution, and entropy of mixing:

$$\delta = (\Sigma\, c_i\, (1-r_i/r)^2)^{1/2} \qquad \text{Equation 1}$$

where δ is the atomic size difference, ci is the atomic percentage of each component, r is the average atomic radius, and r_i is the atomic radius.

$$\Delta H_{mix} = \Sigma\, \Omega\, c_i\, c_j \qquad \text{Equation 2}$$

where ΔH mix is the mixing enthalpy and enthalpy of mixing values for each binary pair (i and j) can be calculated from the Miedema model (Takeuchi and Inoue, 2005)

$$\Delta S_{mix} = -R\, \Sigma\, c_i \ln c_j \qquad \text{Equation 3}$$

where ΔS_{mix} is the entropy of mixing and R is the gas constant.

Guo and Liu (2011) furthered this research by stating that the formation of a solid solution in a high entropy system must require enthalpy of mixing, entropy of mixing, and atomic size difference must be within certain limits: $-22 \leq \Delta H_{mix} \leq 7$ kJ/mol, $11 \leq \Delta S_{mix} \leq 19.5$J/molK and $0 \leq \delta \leq 8.5$.

Further expansion includes utilising the Hume-Rothery rule for valence electron concentration (VEC); a critical parameter which determines whether an FCC (VEC ≥ 8) or BCC phase (VEC < 6.87) will form.

Yang and Zhang, (2012) later defined a new parameter Ω to predict the formation of a solid solution when $\Omega \geq 1.1$ and $\delta \leq 6.6\%$:

$$\Omega = (T_m\, \Delta S_{mix})/\Delta H_{mix} \qquad \text{Equation 4}$$

where T_m is the melting temperature of the alloy using the rule of mixtures approach.

For the BCC-structured elements V, Cr, Mo, and W each parameter was calculated for a range of compositions for each element from 5-35 at%. The most desirable alloy composition minimises the atomic size mismatch whilst ensuring the VEC is below 6.87 and the enthalpy of mixing is between 0 and -5 kJ/mol.

Thermo-Calc

The software Thermo-Calc version 2018b, based on the CALPHAD method, was used to calculate the property diagram of equilibrium phases as a function of temperature. The SSOL4 (SGTE Alloy Solutions Database v4.9g) thermodynamic database was utilised to ensure the binary phase diagrams of the all the elements were taken into consideration. Using the experimentally obtained elemental composition from XRF data, the equilibrium phase diagram of the $V_{2.5}Cr_{1.2}WMoCo_{0.04}$ alloy obtained was plotted between 500 °C and 3000 °C.

Alloy Preparation

The mass of each elemental metal was weighed out for the required composition of a 5g alloy of VCrWMo (all elemental metals sourced from Alfa Aesar with a purity >99.5%). Using a vacuum arc melter (MAM1 Buehler) under a high-purity argon atmosphere with a water-cooled copper hearth and a Ti-getter, a button-shaped ingot was fabricated. Flipping and remelting of the ingot at least five times ensured greater chemical homogeneity.

The alloy was then prepared for irradiation and characterisation using Si-C grit papers up to P2500 followed by polishing solutions and finishing with colloidal silica to ensure a mirror-like finish.

Irradiation

The polished side of the as-cast alloy was implanted at room temperature with 5 MeV Au^+ ions to a fluence of 5×10^{15} Au^+ ions per cm^2 at the Ion Beam Centre in Helmholtz-Zentrum Dresden-Rossendorf, Germany. Using the experimental density measurement, results calculated from the Monte Carlo code SRIM (Ziegler et al., 1985) indicated this implantation condition would produce ballistic damage in a region from the surface to a depth of approximately 800 nm, with a peak damage of about 40 dpa 300 nm below the surface, shown in Figure 1.

Heat Treatment

The as-cast alloy underwent an ageing heat treatment at 1187 °C. This is approximately 0.5 $T_{m,}$ estimated from the experimentally determined elemental compositions from XRF data using the rule of mixtures methodology to provide an estimate of the melting point (Table 1). The alloy was encapsulated in an evacuated silica quartz ampoule to minimise oxidation, heat treated in a box furnace for 500 hours and then quenched in water to preserve the equilibrium phases at the chosen intermediate temperature.

Alloy Characterisation

To determine the crystal structure of the alloy after Au^+ ion implantation, Grazing incidence X-ray diffraction (GI-XRD) was carried out using a PANalytical X'pert^3 Powder diffractometer with Cu Kα radiation operated at 45 kV and 40 mA. For irradiated samples, the X-ray penetration depth was calculated using linear attenuation theory. An incident angle of 1.947° was calculated to probe a depth of 500 nm below the surface, in accordance to SRIM results, so only the near-surface implantation-induced damage region would be probed. To perform phase analysis, the International Centre for Diffraction Data's (ICDD) SIeve+ software was used to search the PDF -4+ database. X-ray fluorescence (XRF) using a PANalytical Zetium spectrometer under vacuum at room temperature with a spot size of 6mm was used to establish the relative elemental composition of the alloy using the PANalytical Omnian analysis software. The microstructure of the alloy was investigated by scanning electron microscopy (SEM), using a Hitachi TM3030 Tabletop SEM, operating at 15 keV, and an FEI Inspect F50 SEM, operating at 20 kV with energy dispersive X-ray (EDX) spectroscopy to detect the elemental distribution within the phases. Vickers microhardness testing was performed on a Bakelite mounted sample in five random locations of the button-shaped alloy. The dwell time was set to 10s, magnification ×40, with a load of 1kg using a Struers DuraScan-70 system. The density of the as-cast alloy was determined using the Archimedes method using a Mettler Toledo NewClassic MF balance.

Results and Discussion

As-cast $V_{2.5}Cr_{1.2}WMoCo_{0.04}$

There was a small contamination of Co in the water-cooled copper crucible in the vacuum chamber during the melting process, with the quantitative analysis of the fabricated alloy by XRF characterisation calculating the composition to be 43.4V-21.75Cr-17.11W-17.11Mo-0.635Co. Throughout this work this is referred to simply as $V_{2.5}Cr_{1.2}WMoCo_{0.04}$.

For the as-cast alloy, SEM and EDX mapping clearly show a multiphase, mostly dendritic, microstructure (Figure 2a1, b1); this can be attributed to elemental segregation on a microscale. During the melting process, the highest melting element (W) solidifies preferentially into the growing dendrites, whilst V and Cr segregate into the inter-dendritic regions. Mo is more homogeneously distributed, with slight preferential distribution to the inter-dendritic regions (Figure 3a). As suggested by Ikeuchi et al. (2019) the preferential segregation of V and Cr is likely to be due to the negative enthalpy of mixing of V-Cr in comparison to the slightly positive enthalpy of mixing between W-Cr and Mo-Cr. The small content of cobalt is clearly segregated from the rest of the melt and precipitates by itself in the inter-dendritic region. For the elements V, Cr, Mo, and W when assessing the binary phase diagrams (Brandes and Brook, 2013) there is a continuous solid solution formation across the entire temperature range with very little formation of intermetallic compounds (only CrW_3 is suggested at potentially forming at 91 wt% of W). The binary phase diagrams for the elements including Co are more complex and suggest the formation of a variety of intermetallic compounds over a range of temperatures and compositions with all the other elements present. This suggests that the removal of cobalt from the alloy would produce very similar results with respect to morphology and crystal structures. The small atomic percentage of cobalt present in the alloy does not appear to play a significant role in the microstructure or have a substantial effect on phase stability and thus is established as a contaminant within the alloy.

As-fabricated $V_{2.5}Cr_{1.2}WMoCo_{0.04}$ displayed a single BCC phase (Finkel et al, 1969) XRD pattern (Table 2) where indexes of the crystal planes of the experimental diffraction peaks corresponds to a lattice parameter a=3.03 Å (Table 1). This matches exactly to the rule of mixtures (Vegard's law – Vegard, 1921) calculated lattice parameter a=3.03 Å. This match is consistent with a random distribution of the elements in a single-phase structure, i.e. the BCC solid solution. Additionally, both density measurements, experimental and theoretically predicted, support that the alloy is likely in a random disordered solid solution state. The small resultant increase in percentage volume, 13.41%, is attributed to the porosity observed in the as-cast alloy, directly formed from the rapid cooling rates induced by the process of arc-melting.

The detection of a single-phase from XRD data (Figure 4) may result from the crystal structures of two (or more) phases being of the same type and very similar in lattice parameter – this is expected as all the pure elements are BCC metals (Table 1) and have similar lattice constants (aside from Co which has an FCC and HCP phase at room temperature) resulting in a less distorted lattice and stable crystal structure. The as-cast XRD pattern displayed narrow peaks but with a slight shoulder on the right-hand side of the peaks at a higher angle indicating a possible overlap of two or more very similar disordered BCC phases. This would coincide with SEM observations and will be further resolved using the sensitivity of neutron diffraction and transmission electron microscopy at a later date.

Confirmation that the BCC phase would be expected can be seen from the Thermo-Calc predictions which show a single ordered BCC phase over a wide temperature range from 750 °C to 2400 °C. Additionally, the presence of two ordered BCC_A2 phases is predicted up to 700 °C (Figure 5). The ROM melting temperature (Table 1) also accurately matches the Thermo-Calc calculation, most likely due to the absence of predicted intermediate phases resulting in a less significant temperature deviation from the ROM value.

Irradiated $V_{2.5}Cr_{1.2}WMoCo_{0.04}$

XRD examination of the post-irradiated $V_{2.5}Cr_{1.2}WMoCo_{0.04}$ revealed a retention of ~96 wt. % of the as-fabricated BCC crystal structure (Figure 4) despite some broadening of the peaks at higher angles. The additional 4wt.% is attributed to the transformation of a second BCC structure with an expansion of the lattice parameter a=3.16 Å. This phase is analogous to W (Gladyshevkii et al, 1967) and is shifted more extensively at higher angles. The retainment of the as-cast crystal structure is somewhat surprising as in conventional alloys, radiation-enhanced diffusion during ion implantation promotes a change in crystal structure. The increase in atomic diffusion during irradiation is due to the enhanced number of defects and the continual creation of new defects. Under irradiation, the concentration of interstitials and vacancies within a material are increased when compared to those produced thermally, which results in diffusion coefficients several orders of magnitude larger than thermal diffusion

coefficients. Enhanced chromium diffusion in austenitic steel alloys is typically observed after ion irradiation, ~4 orders of magnitude higher than that of the thermally annealed sample (Chen et al, 2018), however it is predicted for HEAs that sluggish atomic diffusion may suppress this effect, and this is addressed later in the discussion.

There is no apparent elemental rearrangement or variation in composition in the dendritic and inter-dendritic regions following ion implantation; EDX maps (Figure 3b) of the alloy after irradiation are in good agreement with the as-cast sample further underlining the exceptional phase stability. No radiation-induced segregation (RIS) has taken place due to the ion implantation taking place at room temperature. Normally at elevated temperatures, a redistribution of solute and impurity elements leads to enrichment or depletion of alloying elements near the implantation surface, dislocations, voids, and grain boundaries. Such radical changes can lead to localised property differences and an overall loss in integrity of the component. The stability of $V_{2.5}Cr_{1.2}WMoCo_{0.04}$ could be attributed to the chemical heterogeneity of the single-phase structure in HEAs, which results in the pinning of dislocations (Wu et al., 2016) and reduced thermal conductivity, due to the lattice distortion effect (Xia et al., 2016 and Gao et al., 2016).

Some studies have shown the structural stability on irradiation of single phase HEAs and attributed the irradiation tolerance to high configurational entropy (Murty et al., 2014). Reports so far have stated that multiphase alloys exhibit phase separation and thus are not stabilised against radiation damage by the high entropy effect. In this case the considerable likeness between the two dendritic BCC phase lattice parameters may indicate a two-phase structure, of the type obtained in the alloy under study, is not detrimental to phase stability. Comparable HEA studies displaying results from similar doses of irradiation include Xia et al. (2015) and Yang et al. (2016). $V_{2.5}Cr_{1.2}WMoCo_{0.04}$ can be likened to the HEAs in these reports, $Al_xCoCrFeNi$, which similarly displayed structural stability up to 50 dpa from Au^+ ions at room temperature. With regards to phase stability, the as-cast single FCC phase $Al_{0.1}CoCrFeNi$ HEA demonstrated excellent phase preservation, whereas the as-cast multiphase alloys displayed irradiation-induced defect clusters and precipitation, as observed by TEM studies, upon ion irradiation. This instability upon implantation was credited to the initial phase separation and ordered nature of the multiple phases, causing them to behave like conventional binary and ternary alloys. In the same study, the single-phase as-cast alloys demonstrated no precipitation for doses of 43 dpa. The atomic scale rearrangement in the ion-implanted $V_{2.5}Cr_{1.2}WMoCo_{0.04}$ may not be observed due to the resolution of SEM. As mentioned previously, further TEM studies will reveal if any fine scale precipitation or atomic rearrangement has occurred.

Despite having a multiphase microstructure, the structural phase stability of $V_{2.5}Cr_{1.2}WMoCo_{0.04}$ after irradiation at doses of up to 42 dpa is evident as shown by the SEM micrographs (Figure 2a2, b2). In this report, results gathered from the SRIM simulation (Figure 1) indicate that the maximum radiation damage depth would be at 800 nm below the implantation surface with peak damage of 40 dpa occurring at 300 nm, and a damage level of 10 dpa at the surface. However, there is little difference in the morphology post-irradiation, with structural features also being retained. The average ion penetration of the $Al_{0.1}CoCrFeNi$ alloy was less than 100 nm which was enough to observe by SEM irradiation-induced structural changes. Some HEAs have been found to exhibit structural changes with as little as 1 dpa; equiatomic CrFeCoNiMn and CrFeCoNiPd alloys produced a further L10 phase and spinodal decomposition after 1250 eV electron irradiation (He et al, 2017). Whilst GI-XRD allows for investigation of any implantation-induced structural modifications below the surface, only surface modifications can be detected by the SEM used in this study. SRIM typically overestimates the amount of damage produced, as the simulation assumes the sample to be amorphous, and at absolute zero. Therefore, in reality the level of damage produced at surface may not have been sufficient to cause microstructural changes.

Unlike the single-phase HEAs, where their phase stability has been attributed to their high configurational entropy, as-cast $V_{2.5}Cr_{1.2}WMoCo_{0.04}$ exhibits clear elemental separation yet has still shown excellent phase stability at similar doses to the $Al_xCoCrFeNi$ irradiation studies. This study therefore disagrees with previous reports that only single phase HEAs can demonstrate superior irradiation resistance (Kumar et al., 2016 and Xia et al., 2015) and instead suggests that the stability of the alloy is partly dependent on the particular phases which are present and which phase transformations are likely to occur. As mentioned previously, suppressed atomic diffusion due to lower diffusion kinetics in HEAs has been previously reported in numerous different alloys (Zhang et al., 2014) and this sluggish solute diffusion could be contributing to the suppression of phase transformations. However, as highlighted by reviews on the topic, Pickering and Jones (2016) and Miracle and Senkov (2016), there is not yet enough evidence to clearly demonstrate that atomic diffusion within HEAs is particularly sluggish in comparison to conventional alloys, and it may even be faster. It is unknown whether sluggish diffusion has played a role in the stability, as suggested by Kumar et al. (2016) and Yang et al. (2016), as the ion irradiation study in this report was not conducted at elevated temperatures. In this case, it is proposed that the self-healing effect of HEAs is responsible for the stability of the multiphase alloy.

Based on this hypothesis, the resistance against irradiation is not dominated by the high configurational entropy of this multicomponent alloy, but instead is related to the local distortions within the lattice due to the mismatch of atomic radii. Lattice distortion was termed as one of the 'four core effects' in the original definition of HEAs and was initially based on the hard sphere model, but this has since been deemed an inefficient theory. As determined by Yu et al., the soft sphere model accounts for the atomic stress induced by different elements occupying the same crystallographic lattice site. The local residual strains (comprised of both shear and volumetric components) fluctuate considerably whilst the average value of residual strain is close to zero (Ye et al., 2018). Whilst the atomic radii of each of the elements in V2.5Cr1.2WMoCo0.04 are all similar, the change in atomic radii due to charge transfer and the elastic modulus misfit of the constituent elements causes a residual strain field with strong atomic-level pressures. It is the high atomic level stresses which is hypothesised to be responsible for increasing strength and improving resistance against particle irradiation in this alloy as previously explained by Egami et al. (2015).

Annealed $V_{2.5}Cr_{1.2}WMoCo_{0.04}$

Whilst the as-cast state is mostly stable against phase changes following ion irradiation, upon heat treatment at 1187 °C for 500 hours, a phase transformation occurred with a further three phases being present in the XRD patterns (composed of a tetragonal, an orthorhombic phase, and a BCC phase) indicating the alloy did not consist of equilibrium phases in the as-cast state (Figure 6). The heat-treated BCC phase has a slightly larger lattice parameter (a=3.12 Å) than the phase present in the as-cast alloy (a=3.03 Å) and accounts for 25 wt.% of the microstructure. This is analogous to $Cr_{0.33}W_{0.33}Mo_{0.34}$ (Grum-Grzhimailo and Prokofev, 1961). The tetragonal phase accounts for 24 wt.% of the structure and is isostructural to $V_{0.72}N_{0.28}$ with a lattice parameter of a=9.08 Å and c=4.49 Å (Joubert and Percheron-Guégan, 2001). The majority phase at 51 wt.% is an orthorhombic phase comparable to $Mn_{0.67}N_{0.33}$ with a lattice parameter a=5.67 Å, b=4.91 Å, and c=4.54 Å (Mekata et al, 1968). This unexpected phase transformation, not predicted by the CALPHAD method, is evidence that the as-cast disordered BCC phases were metastable. The validity of the predictive methods employed by Thermo-Calc have been examined for high entropy multicomponent systems. The thermodynamic database selected for the calculation of equilibrium phases is of great importance as this will determine which binary and ternary phase diagrams are used for the Gibbs free energy component of the phase diagram calculation. Contrary to this, Tancret et al. (2017) reviewed a range of databases and their accuracy in predicting stable phases in concentrated alloy space but found there were small discrepancies.

Especially at lower temperatures and of the prediction of smaller concentrations of phases, Thermo-Calc has been shown to not accurately predict phases present experimentally in as-cast alloys, most likely due to the kinetic restraints of the computational method (Manzoni et al., 2015). This demonstrates that, whilst the CALPHAD method can be a useful tool in the high-throughput approach for the exploration of HEAs, care must be taken in accepting the prediction of equilibrium phases.

$V_{2.5}Cr_{1.2}WMoCo_{0.04}$ also exhibited microstructural changes after heat treatment. From the EDX maps (Figure 7) Co is still segregated from the other elements post-heat treatment like both the as-cast state and upon irradiation. Whilst the W-rich dendritic cores remain unchanged, V has diffused out and precipitated in between the dendrites (Figure 8). These V precipitates are attributed to the tetragonal phase detected in the XRD pattern as this structure was analogous to the $V_{0.72}Ni_{0.28}$ phase. Areas of the dendrites which appear to be retained likely consist of Cr-Mo-W according to the EDX maps, and this is expected to be isostructural to the BCC structure $Cr_{0.33}W_{0.33}Mo_{0.34}$ reported from the XRD data. This leaves the remaining inter-dendritic phase, Cr-Mo-Co to be associated with the majority orthorhombic phase. The tetragonal and orthorhombic phases were kinetically restricted during fabrication due to high cooling rates of arc-melting. Furthermore, the proposed slow diffusivity of elements in the multicomponent alloy may have contributed to the suppression of these additional phases. Due to homogenisation of the alloy, the dendritic structure is much less defined and has become globular and more rounded due to the reduction of interface area as seen in the back-scattered micrographs (Figure 8).

The water-cooled copper crucible containing the ingot during fabrication induced rapid cooling which most likely would have suppressed the formation of equilibrium phases, resulting instead in quenched metastable BCC phases forming in the as cast state. This is also supported by the metastable dendritic microstructure as the formation of dendrites commonly occurs from the large undercooling where the melt is in contact with the cooled-copper crucible (although in such complex alloys constitutional supercooling cannot be discounted). For this reason, arc-melted HEAs frequently display dendritic microstructures in their as-cast state (Licavoli et al., 2015).

Precipitation of V at 0.5 T_m was not wholly unexpected as it has been previously proposed that HEAs will decompose into more than one phase upon heat treatment above the solvus temperature (Tsai and Yeh, 2014). Precipitation of further phases at 1187 °C may not be detrimental to its irradiation resistance at application temperatures (for example, claddings of a reactor core do not exceed a peak temperature of 700 °C) but indicates ion irradiation at elevated temperatures is needed if the application temperature is higher. Furthermore, as reported by Pickering et al. (2016), there are several examples of HEAs which form precipitates at intermediate temperatures but demonstrate excellent phase stability at higher temperatures. To assess whether the as-cast phases are either metastable or if further phases are being kinetically restricted, additional prolonged annealing at intermediate temperatures is required. Even though at the intermediate temperature of 1187 °C the alloy underwent a phase transformation, the metastable state of the alloy has shown stability against ion irradiation at room temperature.

Vickers Microhardness

The exceptionally high hardness demonstrated by the as-cast alloy is comparable to many reported HEAs (Dang et al., 2018; Long et al., 2019). In HEAs the atoms are regarded as solute atoms and therefore form saturated solid solutions. This solid solution strengthening effect enhances the strength of these alloys, in comparison to similar conventional alloys, by deterring the motion of dislocations. The multi-phase nature of the alloy would also be expected to contribute to an increase in hardness.

The unexpected decrease in hardness post-irradiation (from 9.47 GPa ± 1.08 to 7.55 GPa ± 0.18 see Table 2) may be further confirmation of the self-healing of radiation-induced defects and intrinsic material defects. Irradiating at low temperatures increases the likelihood of both radiation hardening and embrittlement in high entropy alloys and conventional alloys alike, thus causing a degradation of fracture toughness and increasing the ductile to brittle transition temperature (Victoria et al., 2001). This is a direct result of the defect-damaged microstructure that develops upon irradiation. At low irradiation temperatures ($<0.3T_m$) considerable hardening is predicted to occur due to the increase in irradiation defect clusters including dislocation loops which operate as obstacles to the glide of dislocations (Kumar et al., 2016). And so, a predicted increase in Vickers microhardness is expected to be observed post-irradiation as seen by many irradiated HEAs (Kumar et al., 2016; Yeh et al., 2004; El-Atwani et al., 2019), yet the softening of the alloy can be further evidence of defect recombination, without these other hardening and embrittling effects. According to Egami et al., the recrystallisation of the radiation-induced melt unexpectedly causes a reduction in hardness due to defect recombination 'healing' any intrinsic defects, leading to less mobile dislocations. The phase stability of the alloy suggests that this is not entirely the case for $V_{2.5}Cr_{1.2}WMoCo_{0.04}$. The decrease in hardness is more favourable than embrittlement for structural materials, however the long-term effect of a decrease in hardness is unknown as it is only theorised that self-healing is the responsible mechanism.

A recent study has attributed the decrease of hardness post irradiation at a dose of 1.0×10^{18} He^+ ions per cm^2 to an exfoliation of the surface of CoCrFeCuNi in addition to recovery induced by a long-term thermal spike (Wang et al., 2018). This is consistent with helium ion implantation, where regions of the implantation surface completely detach from the alloy due to the deformation caused by the intersection of helium ions. So, as expected there is no exfoliation of the irradiation layer in $V_{2.5}Cr_{1.2}WMoCo_{0.04}$ upon Au^+ irradiation to account for the decrease in hardness post-irradiation. Instead, the annealing of any defects is most likely responsible for the decrease in hardness post-irradiation.

After heat treatment there was an increase in overall hardness (from 9.47 GPa ± 1.08 to 10.41 GPa ± 0.20) which can be attributed to the precipitation hardening seen from SEM micrographs due to the formation of V precipitates.

Conclusion

The metastable as-cast state of the alloy has shown excellent phase stability against 5 MeV Au^+ ion irradiation of doses up to 42 dpa. SEM micrographs highlight no change in microstructure post-irradiation and EDX maps show no further elemental segregation. In the as-cast state a single BCC crystal structure detected by XRD is speculated to consist of two similar microsegregated disordered BCC phases. GI-XRD has shown that post-irradiation, 96 wt. % of this original BCC structure is preserved with the remaining 4 wt.% phase transforming into a similar BCC phase with a slightly larger lattice parameter. This preservation has been attributed to the self-healing effect due to the multiphase nature of the alloy. Following ion implantation, $V_{2.5}Cr_{1.2}WMoCo_{0.04}$ demonstrated exceptional resistance against radiation hardening and embrittlement which may be due to self-healing and recombination of radiation-induced defects. The formation of three phases, BCC, tetragonal, and orthorhombic in

crystal structure, post-heat treatment indicate that the alloy was only metastable in the as-cast state. However, this metastable state has shown to possess superior irradiation resistance.

The exceptional phase stability of the $V_{2.5}Cr_{1.2}WMoCo_{0.04}$ demonstrates the need for further research into multiphase HEAs and other multicomponent systems due to the uncertainty it raises over previous theories that only single-phase microstructures are desirable for radiation damage tolerant structural components. $V_{2.5}Cr_{1.2}WMoCo_{0.04}$ proves to be a very promising alloy as shown by the resistance to radiation damage and phase stability against ion irradiation.

Acknowledgements

DP would like to acknowledge the financial support of the UK Atomic Energy Authority, funded via the Euratom research and training programme 2014-2018 under grant agreement No 633053 and RCUK [grant number EP/P012450/1] and EPSRC grant EP/L016273 Centre for Doctoral Training in Advanced Metallic Systems for supporting this research. RG would like to acknowledge a Fellowship supported by the Royal Academy of Engineering under the RAEng/Leverhulme Trust Senior Research Fellowships scheme. AG would like to acknowledge funding from EPSRC grant EP/R021864/1. The authors would also like to give special thanks to Dr Zhaoyuan Leong for fabrication of the alloy.

References

Brandes, E.A. and Brook, G.B. eds., 2013. Smithells metals reference book. Elsevier.

Cantor, B., Chang, I. T. H., Knight, P. & Vincent, A. J. B. Microstructural development in equiatomic multicomponent alloys. Mater. Sci. Eng. A 375–377, 213–218 (2004)

Chen, T., Yang, Y., He, L., Tyburska-Püschel, B., Sridharan, K., Xu, H. and Tan, L., 2018. Enhanced diffusion of Cr in 20Cr-25Ni type alloys under proton irradiation at 670° C. Nuclear Materials and Energy, 17, pp.142-146.

Chuang, M.-H., Tsai, M.-H., Wang, W.-R., Lin, S.-J. & Yeh, J.-W. Microstructure and wear behavior of AlxCo1.5CrFeNi1.5Tiy high-entropy alloys. Acta. Mater. 59, 6308–6317 (2011)

Dang, C., Surjadi, J.U., Gao, L. and Lu, Y., 2018. Mechanical properties of nanostructured CoCrFeNiMn high-entropy alloy (HEA) coating. Frontiers in Materials, 5, p.41.

Egami, T., Guo, W., Rack, P.D. and Nagase, T., 2014. Irradiation resistance of multicomponent alloys. Metallurgical and Materials Transactions A, 45(1), pp.180-183.

El-Atwani, O., Li, N., Li, M., Devaraj, A., Baldwin, J.K.S., Schneider, M.M., Sobieraj, D., Wróbel, J.S., Nguyen-Manh, D., Maloy, S.A. and Martinez, E., 2019. Outstanding radiation resistance of tungsten-based high-entropy alloys. Science advances, 5(3), 2002.

Finkel, V., Glamazda, V. and Kovtun, G., Phase Transformation in Vanadium. Zhur Eksper Teoret Fiziki, 1969, 57, 4--10--, 1065-1068.

Gandy, A.S., Jim, B., Coe, G., Patel, D., Hardwick, L., Akhmadaliev, S., Reeves-McLaren, N. and Goodall, R., 2019. High temperature and ion implantation-induced phase transformations in novel reduced activation Si-Fe-V-Cr (-Mo) high entropy alloys. Frontiers in Materials, 6, p.146.

Gao, M. C., Yeh, J.W., Liaw, P. K. & Zhang, Y. High-entropy alloys: Fundamentals and applications. (Springer, 2016).

Gladyshevskii, E.I., Fedorov, T.F., Skolozdra, R.V. and Gorshkova, L.V., 1967. System WV-Si. Soviet Powder Metallurgy and Metal Ceramics, 6(5), pp.406-408.

Grum-Grzhimailo, N.V. and Prokof'ev, D.I., 1961. X Ray Diffraction Analysis of High-Temperature Solid Solutions Of Cr-W-Mo Alloys. Zhur. Neorg. Khim., 6.

Guo, Sheng and Liu, C.T., 2011. Phase stability in high entropy alloys: formation of solid-solution phase or amorphous phase. Progress in Natural Science: Materials International, 21(6), pp.433-446.

Guo, N.N., Wang, L., Luo, L.S., Li, X.Z., Chen, R.R., Su, Y.Q., Guo, J.J. and Fu, H.Z., 2016. Microstructure and mechanical properties of refractory high entropy (Mo0. 5NbHf0. 5ZrTi) BCC/M5Si3 in-situ compound. Journal of Alloys and Compounds, 660, pp.197-203.

He, M.R., Wang, S., Shi, S., Jin, K., Bei, H., Yasuda, K., Matsumura, S., Higashida, K. and Robertson, I.M., 2017. Mechanisms of radiation-induced segregation in CrFeCoNi-based single-phase concentrated solid solution alloys. Acta Materialia, 126, pp.182-193.

He, Q. and Yang, Y., 2018. On lattice distortion in high entropy alloys. Frontiers in Materials, 5, p.42.

Huang, P. K., Yeh, J. W., Shun, T. T. & Chen, S. K. Multi-Principal-Element Alloys with Improved Oxidation and Wear Resistance for Thermal Spray Coating. Adv. Eng. Mater. 6, 74–78 (2004)

Huang, H., Wu, Y., He, J., Wang, H., Liu, X., An, K., Wu, W. and Lu, Z., 2017. Phase-transformation ductilization of brittle high-entropy alloys via metastability engineering. Advanced Materials, 29(30), p.1701678.

Ikeuchi, D., King, D.J.M., Laws, K.J., Knowles, A.J., Aughterson, R.D., Lumpkin, G.R. and Obbard, E.G., 2019. Cr-Mo-VW: A new refractory and transition metal high-entropy alloy system. Scripta Materialia, 158, pp.141-145.

Kombaiah, B., Jin, K., Bei, H., Edmondson, P.D. and Zhang, Y., 2018. Phase stability of single phase Al0. 12CrNiFeCo high entropy alloy upon irradiation. Materials & Design, 160, pp.1208-1216.

Kumar, N. A. P. K., Li, C., Leonard, K. J., Bei, H. & Zinkle, S. J. Microstructural stability and mechanical behavior of FeNiMnCr high entropy alloy under ion irradiation. Acta Mater. 113, 230–244 (2016).

Li, Z., Pradeep, K.G., Deng, Y., Raabe, D. and Tasan, C.C., 2016. Metastable high-entropy dual-phase alloys overcome the strength–ductility trade-off. Nature, 534(7606), p.227.

Liaw, P.K., Egami, T., Zhang, C., Zhang, F. and Zhang, Y., 2015. Radiation behavior of high-entropy alloys for advanced reactors. Final report(No. DOE/NEUP-11-3196). Univ. of Tennessee, Knoxville, TN (United States); CompuTherm, LLC, Madison, WI (United States).

Long, Y., Liang, X., Su, K., Peng, H. and Li, X., 2019. A fine-grained NbMoTaWVCr refractory high-entropy alloy with ultra-high strength: Microstructural evolution and mechanical properties. Journal of Alloys and Compounds, 780, pp.607-617.

Lu, C., Yang, T., Jin, K., Velisa, G., Xiu, P., Song, M., Peng, Q., Gao, F., Zhang, Y., Bei, H. and Weber, W.J., 2018. Enhanced void swelling in NiCoFeCrPd high-entropy alloy by indentation-induced dislocations. Materials Research Letters, 6(10), pp.584-591.

Manzoni, A.M., Daoud, H.M., Voelkl, R., Glatzel, U. and Wanderka, N., 2015. Influence of W, Mo and Ti trace elements on the phase separation in Al8Co17Cr17Cu8Fe17Ni33 based high entropy alloy. Ultramicroscopy, 159, pp.265-271.

Mekata, M., Haruna, J. and Takaki, H., 1968. Neutron Diffraction Study of Antiferromagnetic Mn2N. Journal of the Physical Society of Japan, 25(1), pp.234-238.

Miracle, D., Miller, J., Senkov, O., Woodward, C., Uchic, M. and Tiley, J., 2014. Exploration and development of high entropy alloys for structural applications. Entropy, 16(1), pp.494-525.

Miracle, D. B. & Senkov, O. N. A critical review of high entropy alloys and related concepts. Acta Mater. 1–64 (2016).

Murty, B. S., Yeh, J.W. & Ranganathan, S. High-Entropy Alloys. (Butterworth-Heinemann, 2014).

Nagase, T., Anada, S., Rack, P.D., Noh, J.H., Yasuda, H., Mori, H. and Egami, T., 2012. Electron-irradiation-induced structural change in Zr–Hf–Nb alloy. Intermetallics, 26, pp.122-130

Joubert, J.M. and Percheron-Guégan, A., 2001. Hydrogen absorption in vanadium-and niobium-based topologically close-packed structures. Journal of alloys and compounds, 317, pp.71-76.

Pickering, E. J. & Jones, N. G. High-entropy alloys: a critical assessment of their founding principles and future prospects. Int. Mater. Rev. 61, 183–202 (2016).

Pickering, E. J., Muñoz-Moreno, R., Stone, H. J. & Jones, N. G. Precipitation in the equiatomic high-entropy alloy CrMnFeCoNi. Scr. Mater. 113, 106–109 (2016).

Senkov, O., Senkova, S. & Woodward, C. Effect of aluminum on the microstructure and properties of two refractory high-entropy alloys. Acta Mater. 68, 214–228 (2014)

Tai, K., Averback, R.S., Bellon, P., Ashkenazy, Y. and Stumphy, B., 2012. Temperature dependence of irradiation-induced creep in dilute nanostructured Cu–W alloys. Journal of Nuclear Materials, 422(1-3), pp.8-13.

Tai, K., Averback, R.S., Bellon, P., Vo, N., Ashkenazy, Y. and Dillon, S.J., 2014. Orientation relationship formed during irradiation induced precipitation of W in Cu. Journal of Nuclear Materials, 454(1-3), pp.126-129.

Takeuchi, A. and Inoue, A., 2005. Classification of bulk metallic glasses by atomic size difference, heat of mixing and period of constituent elements and its application to characterization of the main alloying element. Materials Transactions, 46(12), pp.2817-2829.

Tancret, F., Toda-Caraballo, I., Menou, E. and Díaz-Del, P.E.J.R., 2017. Designing high entropy alloys employing thermodynamics and Gaussian process statistical analysis. Materials & Design, 115, pp.486-497.

Tsai, M.H. & Yeh, J.W. High-Entropy Alloys: A Critical Review. Mater. Res. Lett. 2, 107–123 (2014).

Vegard, L., 1921. Die konstitution der mischkristalle und die raumfüllung der atome. Zeitschrift für Physik A Hadrons and Nuclei, 5(1), pp.17-26.

Victoria, M., Baluc, N. and Spätig, P., 2001. Structural materials for fusion reactors. Nuclear fusion, 41(8), p.1047.

Wang, Y., Zhang, K., Feng, Y., Li, Y., Tang, W. and Wei, B., 2018. Evaluation of Radiation Response in CoCrFeCuNi High-Entropy Alloys. Entropy, 20(11), p.835.

Wei, S., He, F. and Tasan, C.C., 2018. Metastability in high-entropy alloys: A review. Journal of Materials Research, 33(19), pp.2924-2937.

Wu, Z., Gao, Y. and Bei, H., 2016. Thermal activation mechanisms and Labusch-type strengthening analysis for a family of high-entropy and equiatomic solid-solution alloys. Acta Materialia, 120, pp.108-119.

Xia, S. Q., Yang, X., Yang, T. F., Liu, S. & Zhang, Y. Irradiation Resistance in AlxCoCrFeNi High Entropy Alloys. JOM 67, 2340–2344 (2015).

Xia, S., Gao, M. C., Yang, T., Liaw, P. K. & Zhang, Y. Phase stability and microstructures of high entropy alloys ion irradiated to high doses. J. Nucl. Mater. 480, 100–108 (2016).

Yang, X. and Zhang, Y., 2012. Prediction of high-entropy stabilized solid-solution in multi-component alloys. Materials Chemistry and Physics, 132(2-3), pp.233-238.

Yang, T., Xia, S., Liu, S., Wang, C., Liu, S., Fang, Y., Zhang, Y., Xue, J., Yan, S. and Wang, Y., 2016. Precipitation behavior of Al x CoCrFeNi high entropy alloys under ion irradiation. Scientific reports, 6, p.32146.

Yeh, J.W., Chen, S.K., Lin, S.J., Gan, J.Y., Chin, T.S., Shun, T.T., Tsau, C.H. and Chang, S.Y., 2004. Nanostructured high-entropy alloys with multiple principal elements: novel alloy design concepts and outcomes. Advanced Engineering Materials, 6(5), pp.299-303.

Zhang, Y., Zhou, Y.J., Lin, J.P., Chen, G.L. and Liaw, P.K., 2008. Solid-solution phase formation rules for multi-component alloys. Advanced Engineering Materials, 10(6), pp.534-538.

Zhang, Y., Zuo, T.T., Tang, Z., Gao, M.C., Dahmen, K.A., Liaw, P.K. and Lu, Z.P., 2014. Microstructures and properties of high-entropy alloys. Progress in Materials Science, 61, pp.1-93.

Zeigler, J.F., Biersack, J.P. and Littmark, U.N.D.U., 1985. The stopping and range of ions in solids. The Stopping and Range of Ions in Matter, 1. <http://www.srim.org/>

Zinkle, S. J. Fusion materials science: Overview of challenges and recent progress. In Physics of Plasmas (2005).

Table 1. Measured elemental composition (in atomic percentage) of the alloy using XRF data. The melting temperature, T_m, lattice constant, *a*, for each pure element in the alloy, as well as calculated and experimental alloy averages. The density of each pure element and calculated density for the alloy is also displayed.

	V (at%)	W (at%)	Mo (at%)	Cr (at%)	Co (at%)	Alloy calc.	Alloy exp.
Elemental composition (at%)	43.4	17.11	17.11	21.75	0.635	-	-
T_m (°C)	1910	3422	2623	1907	1495	-	2277
a (pm)	303	316.5	314.7	291	250	302.65	303
Density (gcm^{-3})	6.11	7.19	10.28	19.25	8.9	9.647	10.94

Table 2. Measured Vickers microhardness values (GPa) and crystal structure of $V_{2.5}Cr_{1.2}WMoCo_{0.04}$ in the as-cast, irradiated, and heat-treated state.

	Vickers Microhardness (GPa)	Crystal structure observed by XRD
As-cast	9.47± 1.08	Single BCC phases
Irradiated	7.55± 0.18	Two BCC phases
Heat treated	10.41± 1.20	BCC, tetragonal, and orthorhombic

Figure 1: Damage profile calculated using the SRIM code

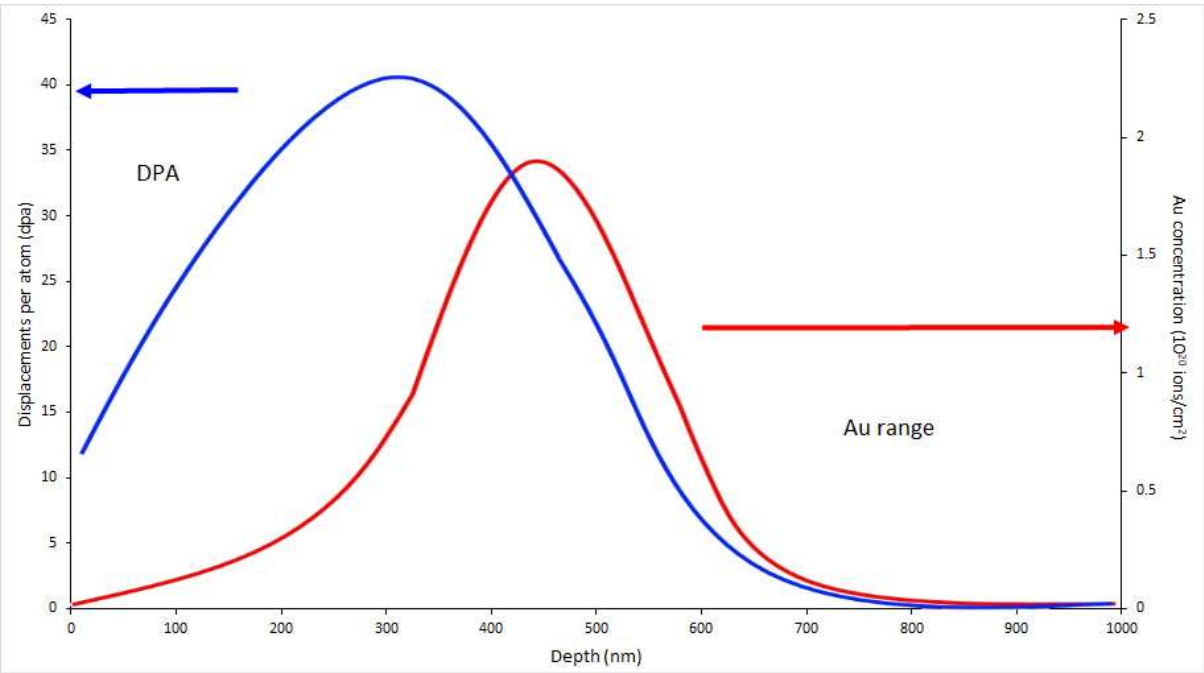

Figure 2: (a1, b1) Backscattered electron images of different regions in as-fabricated $V_{2.5}Cr_{1.2}WMoCo_{0.04}$, (a2, b2) showing the same regions after 5 MeV Au^{+} ion irradiation depicting that no microstructural changes have taken place. The post-irradiation alloy still displays the same dendritic microstructure, indicating stability of the elemental segregation of the as-cast state.

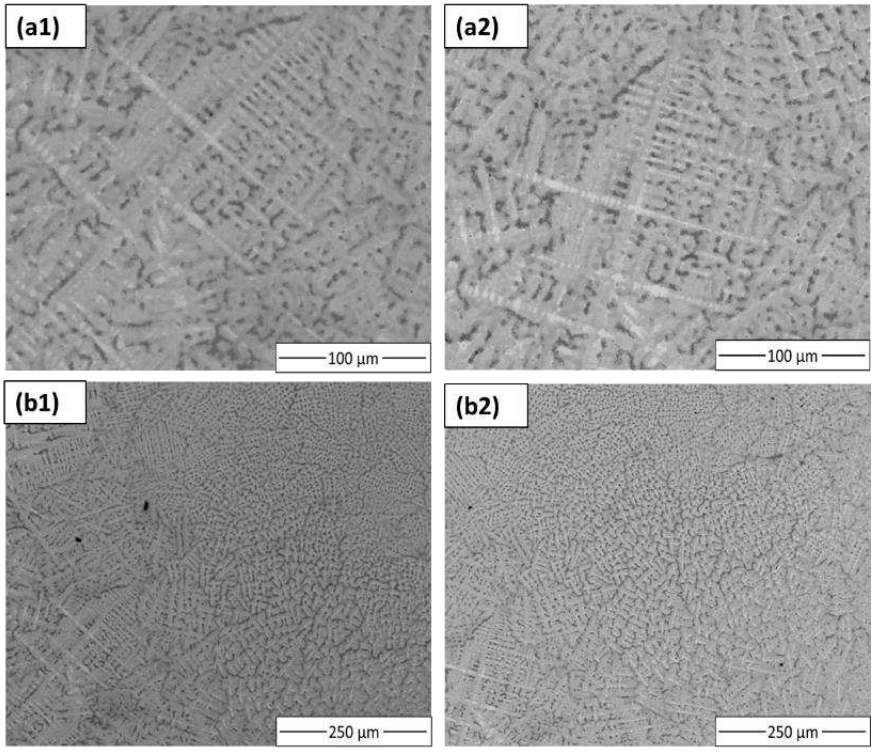

Figure 3: BSE image and EDX maps of the same region in (a) as-fabricated and (b) irradiated $V_{2.5}Cr_{1.2}WMoCo_{0.04}$

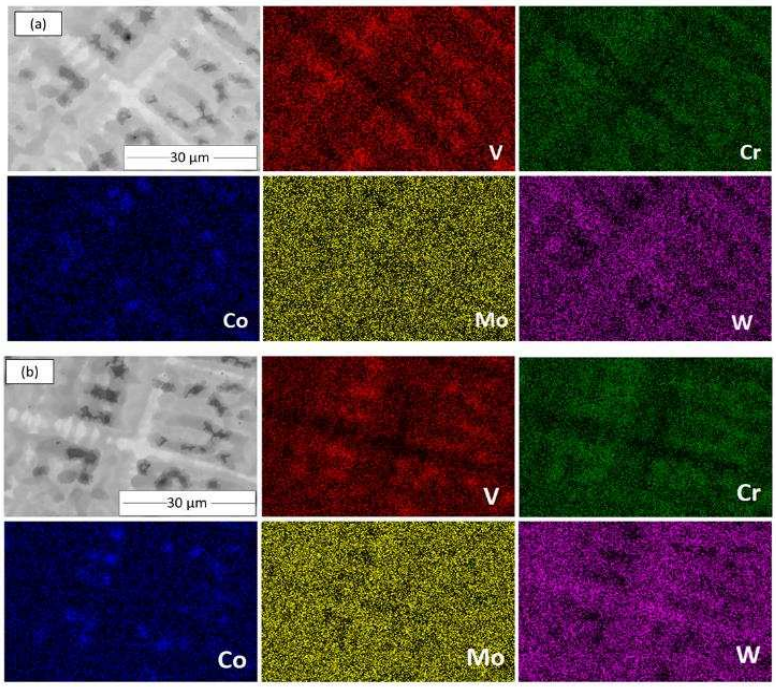

Figure 4: XRD patterns of as-cast $V_{2.5}Cr_{1.2}WMoCo_{0.04}$ and 5 MeV Au^{+} ion irradiated $V_{2.5}Cr_{1.2}WMoCo_{0.04}$. The filled and unfilled circles denote the two BCC phases present in irradiated $V_{2.5}Cr_{1.2}WMoCo_{0.04}$, where the red filled circle denotes the as-cast BCC phase mostly retained post-irradiation.

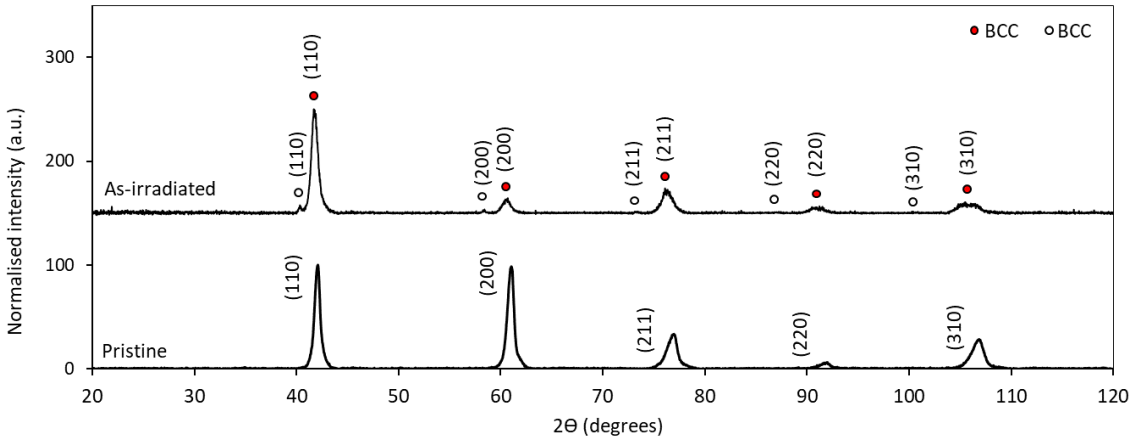

Figure 5: Predicted Thermo-Calc property diagram, indicating the formation of two ordered BCC_A2 phases to be present in $V_{2.5}Cr_{1.2}WMoCo_{0.04}$. The first BCC_A2 phase to be formed is stable over a wide range of temperatures, indicating a single-phase is likely to be present in the alloy.

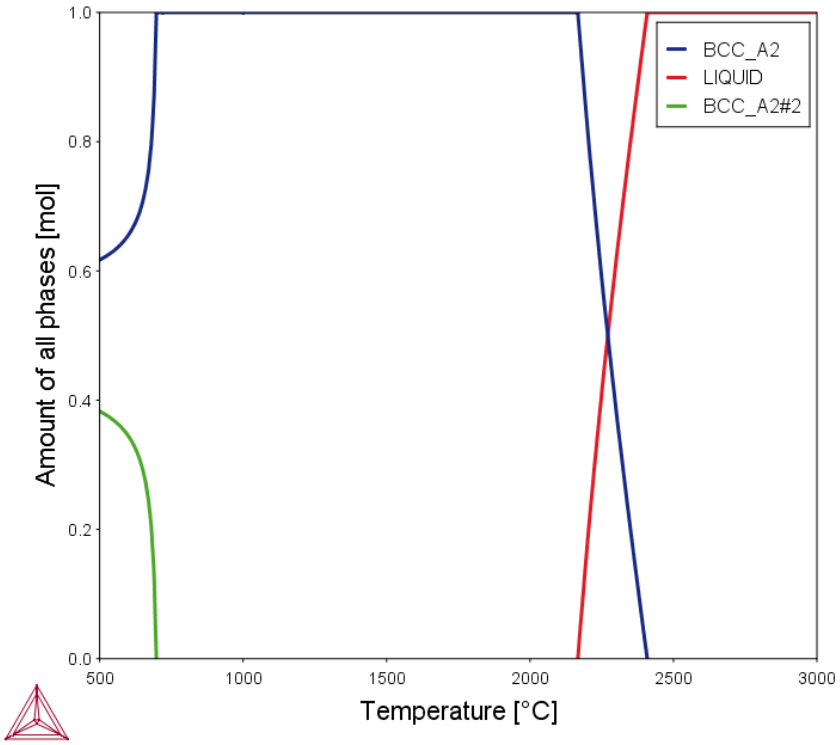

Figure 6: XRD patterns of as-fabricated $V_{2.5}Cr_{1.2}WMoCo_{0.04}$ and heat-treated$V_{2.5}Cr_{1.2}WMoCo_{0.04}$ (1187 °C for 500 hours). The circles, squares and triangles above heat-treated $V_{2.5}Cr_{1.2}WMoCo_{0.04}$ correspond to the BCC, tetragonal, and orthorhombic structures of the phases present.

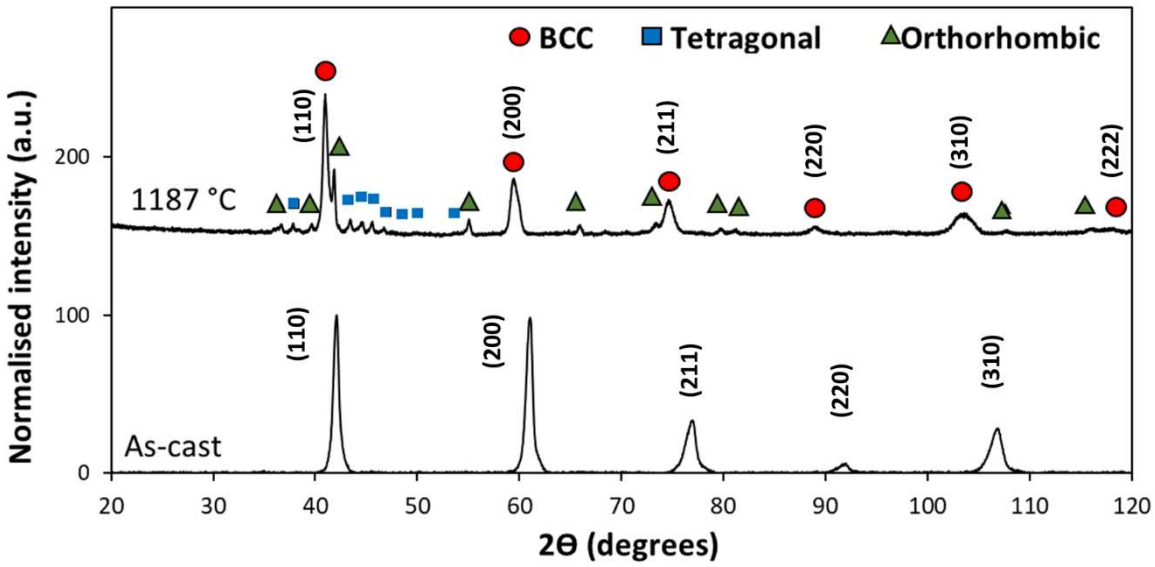

Figure 7: BSE image and EDX map of the heat treated $V_{2.5}Cr_{1.2}WMoCo_{0.04}$

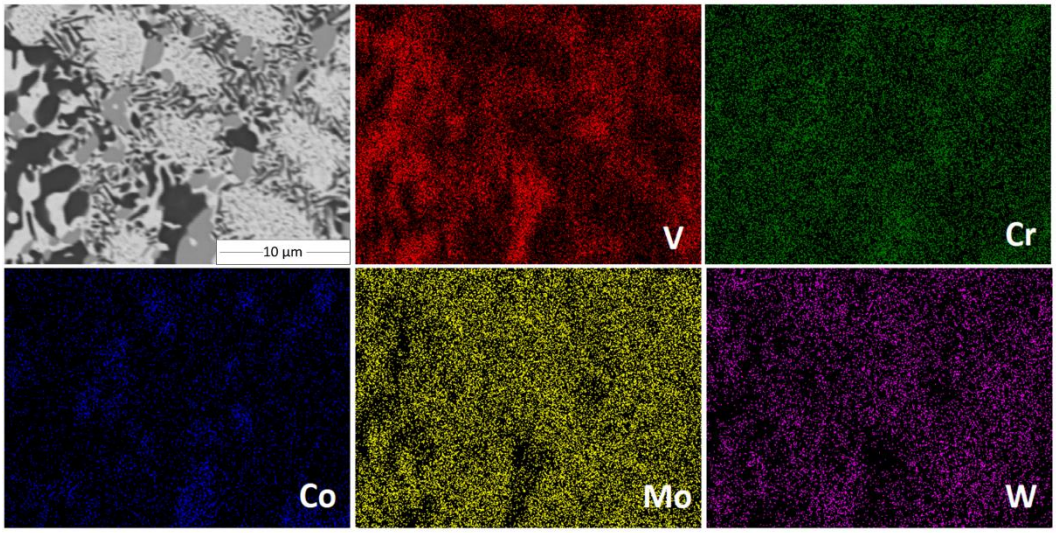

Figure 8: BSE images of different regions in pristine $V_{2.5}Cr_{1.2}WMoCo_{0.04}$, (a1, b1) comparable regions to those in (a2, b2) respectively after heat treatment for 500 hours at 1187 °C.